Dynamics Studies of a Malachite Green−RNA Complex Revealing the Origin of the Red-Shift and Energetic Contributions of Stacking Interactions

Dat H. Nguyen,*,† Thorsten Dieckmann,‡ Michael E. Colvin,§ and William H. Fink*,‡

Department of Genetics, Harvard Medical School, Boston, Massachusetts 02115, Department of Chemistry, University of California, Davis, California 95616, and Schools of Natural Sciences and Engineering, University of California, Merced, California 95340

Received: October 29, 2003

RNA plays a central role in many biological processes and is therefore an important target for drug development. In recent years an increasing wealth of structural and functional information about RNA−ligand complexes has been obtained using in vitro selected RNAs (aptamers). However, all those studies focused on structure and changes of the nucleic acid and mostly considered the ligand as a rigid target. Experimental characterization of the dynamics of a malachite green (MAG)−RNA aptamer complex revealed surprisingly asymmetric changes in the ^{13}C chemical shift of the ligand methyl groups, which indicate that the dye undergoes changes in its conformation and charge distribution upon binding, in addition to the red-shift in its maximum absorption frequency. Earlier computational work explored the electrostatic influence of the highly charged RNA backbone and surrounding counterions for these asymmetrical changes in ^{13}C chemical shift. The work presented here examines the dynamical nature of the MAG molecule inside the RNA ligand-binding site using molecular dynamics with explicit solvent to explore the intermolecular and dynamic influences on the red-shift and to calculate the binding affinity. An induced fit behavior, similar to that caused by the electrostatic field alone, is observed. The binding strength of a series of malachite green derivatives correlates with the structural flatness of the ligand. These findings are important for the rational design of RNA ligands and for understanding the properties of RNA−ligand complexes.

Introduction

The interactions between ribonucleic acids and small molecule ligands play a crucial role in living cells. Recent studies have shown that small molecule effectors can bind directly to RNA switches to regulate biochemical pathways.[1−3] The central role of RNA in many biological processes makes it an attractive target for the design of new drugs that target viral infections or cancer.[4,5] To facilitate the rational design of new ligands that specifically target RNA it is necessary to analyze the structures of RNA−ligand complexes and to identify the intermolecular forces that determine complex affinity and specificity. Numerous RNA−ligand complex structures have been determined in the past 6 years using NMR spectroscopy and X-ray crystallography.[6−8] Many of these studies used in vitro selected RNAs, so-called aptamers,[9] as model systems. The mode of recognition found in most complexes between RNA and small molecules is rather unusual and very different from most proteins: the ligand acts as a scaffold for folding the RNA into an intricate three-dimensional structure and becomes an integral part of the structure. This mode of recognition has been termed "ligand-induced folding" or "adaptive binding" and has been observed in most small molecule binding RNAs characterized to date.[10,11] For example, the structure of the ATP-binding RNA aptamer illustrated that the ligand is recognized via a network of hydrogen bonds and stacking interactions.[12] The binding pocket of the free RNA is very dynamic and largely unfolded and converts into a well-defined structure only in the presence of ATP or AMP.

The malachite green binding RNA aptamer was developed by in vitro selection[13] and not only binds to malachite green (MAG) but also to other MAG-related organic dyes (Figure 1) such as tetramethylrosamine (TMR) and Pyronin Y (PY) with dissociation constants of 800, 40, and 225 nM, for MAG, TMR, and PY, respectively.[13,14] The X-ray structure of the RNA aptamer forming complex with the TMR has been determined by the work of Baugh et al.,[14] and the NMR structure of the RNA aptamer forming complex with the MAG has been determined in one of our laboratories.[15] These studies have shown that the RNA ligand-binding site that houses either MAG or TMR is very similar, as these dyes are stacked between the G8·C28 Watson−Crick base pair and the C7·G24·G29·A31 base quadruple (Figure 1a), although there are some small structural differences due to the fact that TMR contains a large planar ring system whereas all three rings in MAG are rotated relative to each other. Figure 2 illustrates the MAG−RNA complex derived from the experimentally determined X-ray crystal structure[14] TMR−RNA complex by superimposing the MAG structure onto the TMR structure followed by the removal of the TMR molecule from the complex.

Upon formation of a complex with the RNA aptamer, the four symmetrically equivalent *N*-methyl groups of the MAG molecule become asymmetrical as manifested by their chemical shifts shown previously (Figure 2 in ref 16). At the same time, the binding also causes a red-shift in the maximum absorption frequency by 14 nm (from 616 to 630 nm). To help distinguish

* To whom correspondence should be addressed. E-mail: dnguyen@hms.harvard.edu (D.H.N.); fink@chem.ucdavis.edu (W.H.F.).
† Harvard Medical School.
‡ University of California at Davis.
§ University of California at Merced.

10.1021/jp037273b CCC: $27.50
Published on Web 12/25/2003

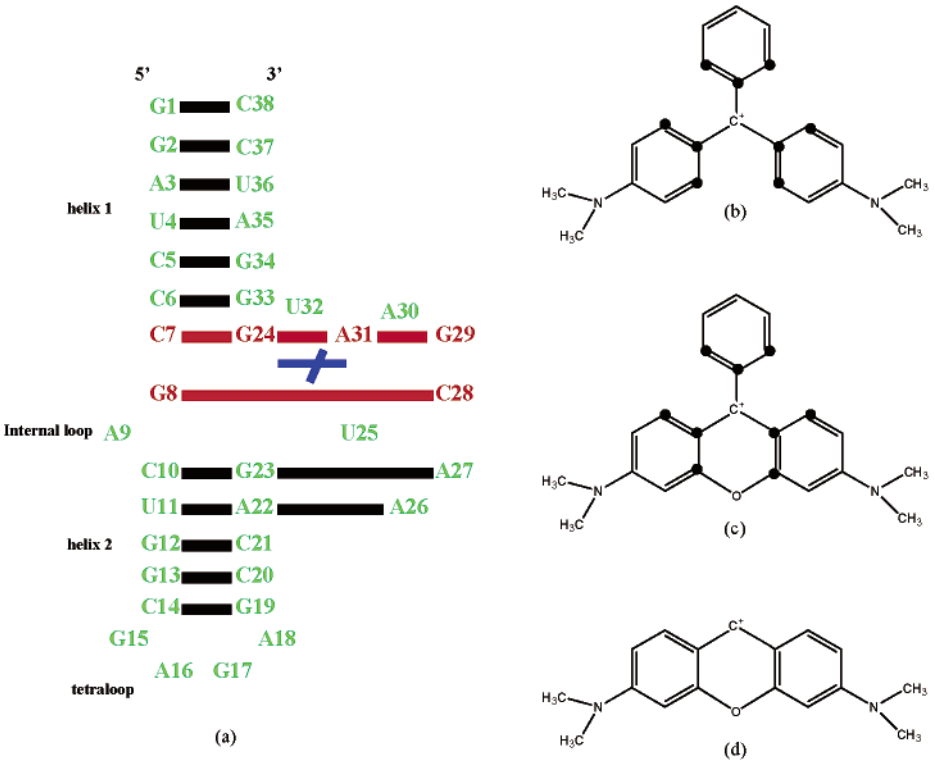

Figure 1. MAG−RNA aptamer complex and related organic dyes: (a) the sequence and structure of MAG−RNA aptamer; (b) malachite green (MAG); (c) tetramethylrosamine (TMR); (d) pyronin (PY). Filled black circles identify atoms used in defining dihedral angles between rings.

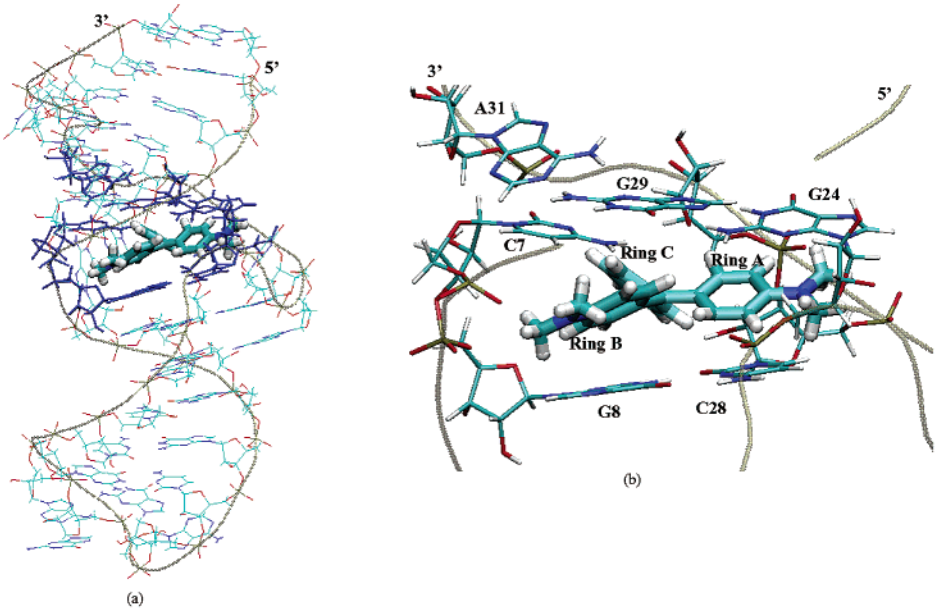

Figure 2. Malachite green in the RNA aptamer ligand binding site: (a) the overview structure of MAG−RNA aptamer complex; (b) the expanded view of the ligand binding site.

the two geometrically symmetrical N-methylated rings on the dyes shown in Figure 2, they are referred to as rings A and B. Ring A is deeply buried inside the ligand-binding pocket, stacked among G24, C28, and G29. When bound to RNA, these *N*-methyl groups on ring A are nonequivalent and show distinctively different NOE patterns at short NOESY mixing times (80 ms).[15] In contrast to this observation, ring B, stacked between C7 and G8, shows clear evidence for a faster rotation of the phenyl ring and the methyl groups on the NMR time scale. The NOE patterns for both methyl groups and the protons on both sides of the ring are identical. The ^{13}C NMR spectrum of free MAG shows only one signal for the four methyl groups (46.2 ppm). Upon binding, four signals are found at 40.3 ppm for ring B and at 39.7 and 36.2 ppm for ring A.[16] Our previous computational work showed that the upfield shift of the *N*-methyl carbon resonances of ring A is indicative of an increased positive charge on ring A as would be expected in the case of a greater contribution of the MAG resonance structure with a charge on the A ring nitrogen. This shift toward a structure with a greater partial charge on the ring A nitrogen

is also consistent with the observation of a hindered rotation of the ring and *N*-methyl group due to the partial double bond character of the bonds connecting the nitrogen to the ring and the ring to the central carbon.

The physical understanding of the molecular basis of interactions between small molecules and RNA aptamer is crucially important for understanding the molecular recognition and folding mechanism of RNA induced by these small molecules. Given that objective, this work is designed to be an examination of interactions between the malachite green molecule and RNA aptamer, using an AMBER molecular dynamics simulation in explicit waters to explore dynamic influences, following up on our previous work,[16] where only electrostatic effects on the electronic structure were considered. As mentioned in this previous paper, the underlying physical nature of interactions between malachite green and the RNA aptamer can be approximately partitioned into two major classes of interaction: electrostatic and extended π-system base-stacking forces. The former interactions arise from a highly charged RNA backbone and surrounding counterions with the positively charged MAG, whereas the latter are the result of interactions between the RNA bases and the aromatic rings of MAG. In our previous work using ab initio electronic structure methods, we determined that the electrostatic interactions exerted by the highly charged RNA backbone and surrounding counterions onto the electronic structure of malachite green molecule caused the asymmetrical chemical shifts of four symmetrical *N*-methyl groups as observed in the NMR experiment. In the present work, we undertake molecular dynamics simulations with explicit solvent to gain insight into the nature of the remaining interactions (and consequently the dynamics) on the red-shift in the maximum absorption frequency and the binding affinity of the malachite green molecule. In particular, we examine the conformational dynamics of the MAG molecule, in terms of the interplanar dihedrals of its aromatic rings both in the presence and absence of the RNA aptamer, as well as its spatial dynamics, in terms of base-stacking energy within the RNA ligand binding site. These interactions are examined because they may be presumed to have an influential role on the red-shift in the absorption frequency and the binding strength of the MAG molecule upon forming a complex with the RNA aptamer. They promote the formation of the extended π-system among rings of the MAG molecule and base stacking energy between rings of the MAG and bases of the RNA aptamer.

Methodology

The goals of this study are two-fold. First, to determine the origin of the red-shift in the maximum absorption frequency of MAG upon binding to RNA aptamer, we examine the conformational dynamics of the MAG molecule (in terms of the coplanarity between rings) in an explicit solvent environment with and without the RNA aptamer. We use the statistically determined potential of mean force (PMF)[27] to examine the characteristic values of the ring dihedrals over the trajectory. Second, to determine the relationship between the conformational dynamics and binding affinity of the MAG, we compare its binding free energy and ring−base stacking energy with the corresponding energies for TMR, since TMR is structurally more planar and binds more strongly to RNA aptamer than the MAG molecule. We use the MM-PBSA method to determine the binding free energy of MAG and TMR to the RNA aptamer and use the Lennard-Jones van der Waals contributions to the AMBER force field to examine ring to base stacking contributions.

Three systems of RNA complexes were simulated in this study: (1) a MAG−RNA complex, starting with a structure determined by NMR spectroscopy;[15] (2) a MAG−RNA complex, starting with an RNA structure derived from an X-ray crystallographic structure for the TMR−RNA complex but with MAG inserted in place of the TMR; (3) a structure starting with the entire TMR−RNA complex determined by crystallography.[14] The second simulated system above was derived from the TMR−RNA complex by superimposing the vacuum-optimized MAG molecule onto the TMR position in the TMR−RNA complex[14] using Kabsch's algorithm[17,18] followed by the removal of the TMR molecule from the complex. The motivation for studying the MAG−RNA complex structures derived from two starting structures is to determine the sensitivity of the computed results to the details of the initial structure. Each of these three complexes was placed into a box of ~5400 TIP3P water[19] with dimensions of $78 \times 58 \times 51$ Å^3 and neutralized by Na^+ counterions. A total of 5000 iterations of conjugate gradient minimization were carried out followed by 220 ps of molecular dynamics to equilibrate each system. Each MAG− and TMR−RNA aptamer complex was then run for 10 ns of MD simulation time. In addition to these three aptamer complex systems, we also ran three additional MD simulations: the unbound RNA aptamer (starting with the X-ray crystal structure of the TMR bound complex but with TMR simply removed in ~5400 TIP3P waters), MAG, and TMR molecules in water (~1000 water molecules) for 2.5 ns of simulation time. These additional simulations are needed for computing the binding free energy and for comparing conformational dynamics of unbound dyes. For all simulations, unconstrained dynamics (i.e. all atoms are allowed to move freely) and the NPT ensemble were employed. The pressure was maintained at 1.0 atm using isotropic scaling with the relaxation time of 1.0 ps, while the temperature was maintained at 300 K using Berendsen's algorithm,[31] and the motion of the center of mass of the simulation system was removed roughly every 0.5 ns. The molecular dynamics was carried out using the AMBER 6.0 program package[20] with Cornell '94 all atom force field.[21] The particle−mesh Ewald algorithm[22] was used for handling long-range electrostatic forces, while the short-range van der Waals force was truncated at 12.0 Å. In the PME, the grid size of ~1.0 Å was used in conjunction with an Ewald coefficient of 0.22 Å^{-1} and an error tolerance of 10^{-5}. The time step was set to 2.0 fs, and the SHAKE algorithm[23] was used to restrain all bonds containing hydrogen atoms with the SHAKE geometrical error tolerance set to 10^{-4} Å. The trajectory was collected as a series of snapshots saved every 2.0 ps. The binding free energy was computed using the MM-PBSA method,[24,25] and the details of parameters used in the MM-PBSA method were previously reported.[26,32] The PMF plots were obtained by examining the values of the dihedral angles for the saved snapshots and accumulating the number of occurrences of each angle in bins of 4° wide. The accumulations were normalized and the relative energies of the bins inferred from the Boltzmann distribution.

Results and Discussion

In this section, we first present the conformational dynamics of MAG and TMR molecules both in the presence and absence of the RNA aptamer so that the effect of the RNA aptamer on the structural dynamics of each of these two dyes can be extracted. The variable used for measuring the conformational dynamics is the dihedral angle between two specified ring planes of interest. We choose this description of the conformational dynamics of the dyes, since it is directly related to the maximum

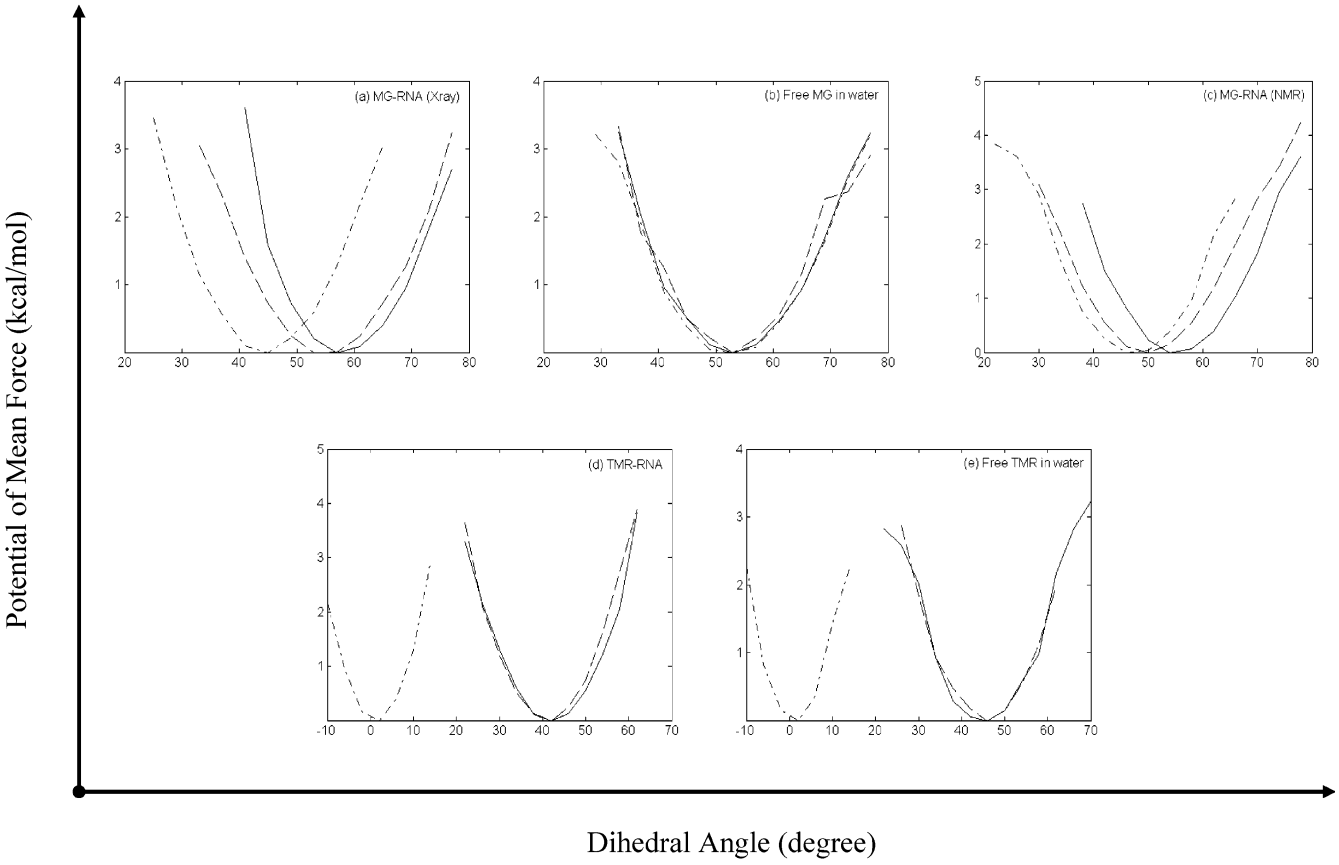

Figure 3. Potential of mean force (PMF) as a function of dihedral angle for each ring pair of both MAG (labeled above as MG) and TMR molecules in different environments. In the computation of the PMF, the bin size of 4° was used, and the distribution of each bin was normalized to the bin with the largest distribution, which is set to be the reference zero-free energy level. Dash−dot, dash−dash, and solid lines denote the potential of mean force of dihedral angles of rings A−B, A−C, and B−C, respectively.

absorption frequency of dyes. Dihedral angles that lead to coplanar aromatic rings in the MAG cause formation of an extended π-system lowering the $\pi-\pi^*$ transition energy and hence leading to a red-shift in the maximum absorption frequency. Second, we present the detailed analyses of binding affinities (in terms of spatial dynamics) for both MAG and TMR to the RNA aptamer to gain more insight into the nature of differential binding affinity of MAG and TMR molecules.

The conformational dynamics of both MAG and TMR molecules can be characterized by their potential of mean force (PMF)[27] along the dihedral angle of two specified ring planes of interest (e.g. dihedral angles between rings A−B, A−C, and B−C and the values quoted for these ring angles are measured using the dihedral angle formed by the meta and ortho carbons on adjacent rings). Figure 3 shows the PMF of both MAG and TMR molecules in bound (in the RNA aptamer) and free (in pure water) environments. As is clear in Figure 3, all rings of free MAG in water experience equivalent torsional potentials with equivalent equilibrium ring interplanar dihedrals of 53°, whereas the equilibrium dihedral angles among the three rings are displaced from each other upon forming a complex with RNA. In the pocket of the RNA aptamer, the MAG molecule adopts a conformation with dihedral angle between rings A and B of 45° (Figure 3a) or 46° (Figure 3c) for complexes determined by the X-ray or NMR, respectively, in contrast to the conformation adopted in pure water with a dihedral angle of 53° (Figure 3b). Although the RNA aptamer ligand-binding environments in the structures determined by NMR and X-ray crystallography are not identical, in both environments the MAG molecule exhibits almost the same PMF profiles and relative orientations of its three rings. In particular, the MAG adopts a more coplanar conformation of its rotatable rings, as measured by a lower value of the dihedral angles, than that seen for the MAG alone in water. As a result, the MAG molecule in the RNA aptamer should exhibit a red-shift in its maximum absorption frequency due to its more highly extended π-system, as was seen previously in our CIS calculations.[16] We note that the details of which rings become more coplanar vary whether examining the results of the electronic structure calculations perturbed by the field of the RNA backbone or the molecular dynamics simulations reported here; however, enhanced overall coplanarity is a theme common to both treatments. These results suggest that the origin of the red-shift in the maximum absorption frequency of the MAG molecule upon forming a complex with the RNA aptamer is from a greater coplanar conformation that the MAG molecule adopts that is induced by the RNA aptamer. The same induced effect of the RNA aptamer is further observed for the TMR molecule, as it also adopts a greater coplanar conformation by shifting values of its dihedral angles between rings A−C and B−C a few degrees lower, although the shift is less significant than for the MAG molecule.

The nature of interactions of both MAG and TMR molecules with the RNA aptamer that determine the binding strength can be probed by calculating the base-stacking energy between each ring of the dye and bases of the RNA. The base-stacking energy depends exclusively on the geometrical alignment of aromatic rings in such a way that allows dispersive interactions between the π-clouds on the aromatic rings of the dyes and the RNA bases.[28] However, we cannot directly compute the base-stacking

TABLE 1: Energy of Interactions of Dyes and RNA Aptamer

		MAG−RNA (X-ray)	MAG−RNA (NMR)	TMR−RNA
van der Waals ring−base-stacking energy (kcal/mol)	ring A	−5.984	−7.161	−5.578
	ring B	−6.476	−6.288	−5.789
	ring C	−6.041	-4.417	−8.061
	total (A + B + C)	−18.501	−17.866	−19.428
Binding free energy (kcal/mol)	computed[a]	−8.166		−17.601
	expt[b]	−8.365		−10.150

[a] See Appendix A (Supporting Information). [b] Values were computed from the dissociation constants: $\Delta G = RT \ln(K_d)$.

energy using classical mechanics since the dispersive component of base-stacking energy is fundamentally a quantum mechanical property that can only be empirically approximated. The high-level first-principles quantum chemical methods necessary to accurately model such dispersive interactions cannot be applied due to the MAG−RNA aptamer's large size. We can nevertheless approximate these dispersive interactions using the empirically derived expressions for the van der Waals interactions between rings of the dye and bases of the RNA molecule. Even if the precise magnitude of the dispersive interactions are not accurately predicted, we expect that the actual π-stacking energy will be well-correlated with these computed energies, since the same geometries that lead to large van der Waals interactions between the dye rings and RNA bases will also lead to high stacking energies, as shown in the recent experimental and computational works by Guckian et al.[29] and Sinnokrot et al.,[28] respectively.

Table 1 presents van der Waals ring−base interactions for each ring of MAG and TMR molecules to all bases of the RNA aptamer averaged over the course of 10 ns dynamics. From the van der Waals energy perspective, the rings of MAG and the corresponding ones of TMR are identical, since they possess the same set of van der Waals parameters. As a result, a direct comparison between the predicted energies of the van der Waals ring−base interactions of the MAG and that of the TMR is meaningful. As shown, the total computed van der Waals ring−base interactions of the TMR molecule (−19.4 kcal/mol) to bases of the RNA aptamer are more favorable than that of the MAG molecule (−18.5 kcal/mol) by ∼0.9 kcal/mol. This computed difference in the van der Waals interactions accounts for about 50% of the 1.8 kcal/mol difference in the experimental binding free energies between MAG and TMR. Table 1 also presents the computed binding free energies for both MAG−RNA and TMR−RNA complexes using the MM-PBSA method where they are compared with the experimental values obtained from the binding constants. The breakdown into individual contributions to the binding energy by the MM-PBSA method has been included in Appendix A (Supporting Information). The extremely fortuitous agreement between computed and experimental binding free energies for the MAG complex is not seen to carry over to the TMR complex, however. The excessive binding computed for the TMR complex may arise from its more compact structure in comparison with the MAG complex simulation. This structural compactness is clearly the origin of the relatively high electrostatic contribution to the molecular force field E_{mm} term of the binding energy (Table A2; Supporting Information). From these relative energies we conclude that increased planarity of the dye molecules leads to stronger binding affinity the RNA aptamer and hence that the binding to the RNA aptamer will induce greater coplanar conformation. Combined with our earlier quantum chemical treatment,[16] this suggests that the coplanarity of the MAG rings induced by binding to the RNA aptamer contributes to the observed red-shift in the maximum absorption frequency.

Further detailed analyses of the van der Waals ring−base interactions of each ring of the MAG molecule to each base of the RNA aptamer yield a description of the spatial dynamics of the MAG molecule in the RNA ligand binding site. Figure 4 presents the computed van der Waals energy of ring−base interactions for each ring of MAG molecule with each base of the RNA aptamer averaged over 10 ns of MD trajectory. Panels a and b in this figure identify the ligand-binding sites in the RNA to which the rings of the dyes are preferentially attractive for the two different starting RNA structures: (a) that derived from the X-ray crystal structure of the TMR−RNA complex; (b) that obtained by NMR directly on the MAG−RNA complex. Inside the RNA aptamer, the spatial dynamics of the MAG molecule in these two different starting environments are strikingly similar as ring A is spatially attractive to C24, C28, and G29, ring B to C7, G8, and G29, and ring C to G29 and A30, although there exist differences in terms of their interaction strengths. Despite these differences, an overall comparison of the MAG−RNA interactions resulting from these two starting configurations yields a consistent picture. If these two experimentally determined RNA aptamer structures are treated as two different initial configurations for the dynamical trajectory, under the ergodic theorem they cover a wider range of conformational sampling space amounting to 20 ns of dynamics. Panel c of Figure 4 shows the composite average of van der Waals ring−base interactions between rings of the MAG molecule and bases of the RNA aptamer over these two trajectories. This figure clearly suggests that rings A and B are intercalated in the space encapsulated by the C7•G29 and G8•C28 Watson−Crick base pairs, which is consistent with the NMR observations.[15] The agreement of the results between the simulations starting from a superposition of MAG into the X-ray structure of the TMR complex with those starting from the actual NMR-derived structure of the MAG−RNA complex helps to validate the superposition procedures. Note that, for the van der Waals ring−base interactions to be meaningful as the base-stacking energy, the magnitude of the van der Waals energy must be significant enough to account for the ring−base geometrical alignment. In this discussion, we chose a threshold arbitrarily at 150% of the thermal energy at 300 °C (0.89 kcal/mol).

The stability or persistency of these spatial modes of van der Waals ring−base interactions between the MAG molecule and the RNA aptamer is analyzed using the so-called "statistical inefficiency" method (see Appendix B; Supporting Information). The statistical inefficiency analyses were done for dominant modes of attraction between MAG rings and RNA bases. As mentioned in Appendix B, the statistical inefficiency method is useful for computing a persistence time of a property of a trajectory, where all data points are generated sequentially. The persistence time can be used to assess the duration of a particular mode of interaction over the entire trajectory. Figure 5 shows plots of the statistical inefficiency *s* as a function of block size (number of snapshots) for each dominant spatial mode of van der Waals ring−base interactions between the MAG molecule

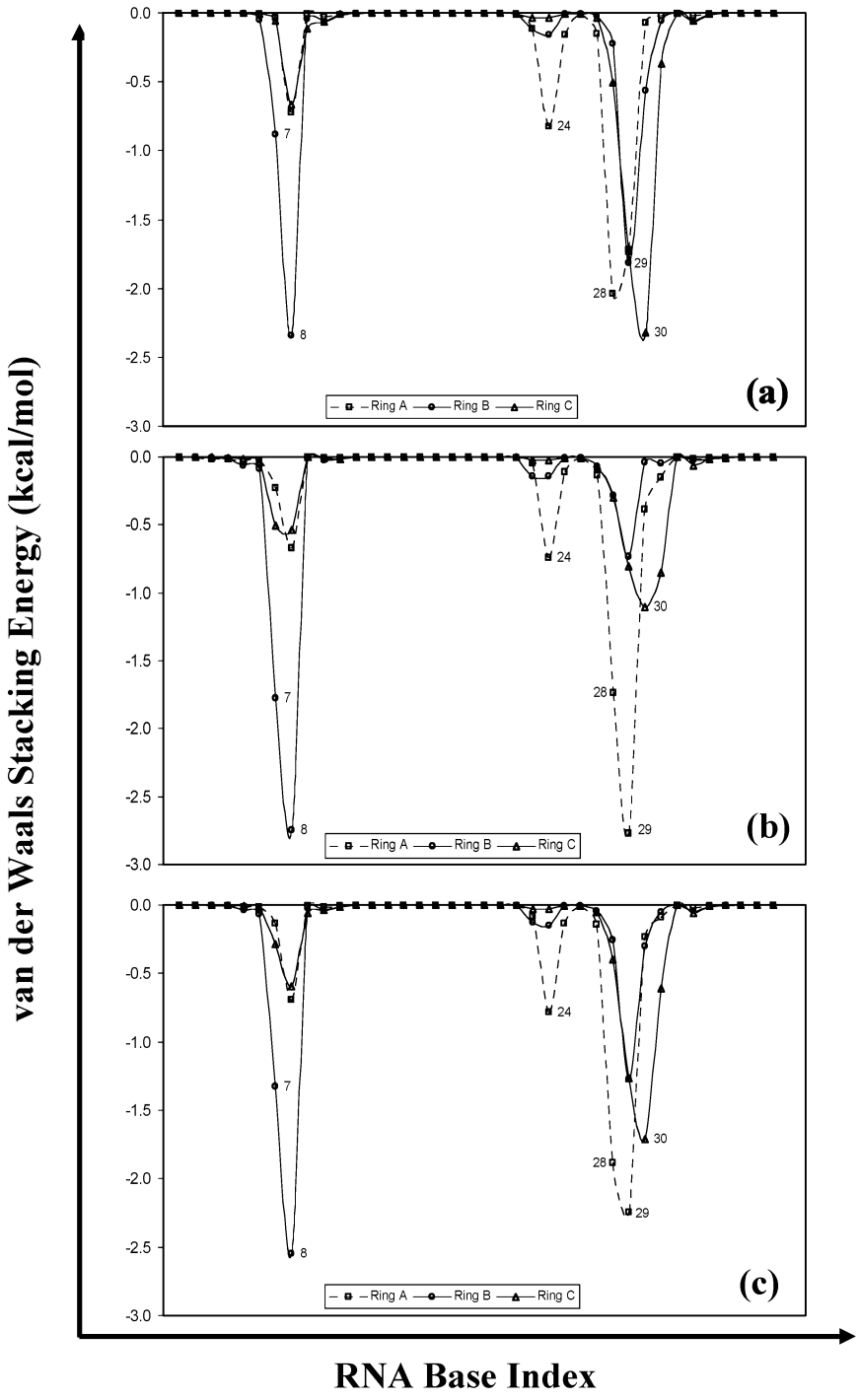

Figure 4. van der Waals ring−base stacking energy (see text for definition) between each ring of the MAG molecule and all bases of the RNA aptamer. Panels a and b show the ring−base interaction results using X-ray crystallography and NMR RNA aptamer structures, respectively. Panel c is a composite average of both panels a and b.

and the RNA aptamer (shown in Figure 4, panels a−c). In the X-ray structure case (panels a−c in Figure 5), the plateau value (from which the persistence time is derived) of each ring does not apparently exist, suggesting that the persistence time of these spatial attractive modes is longer than the dynamical time period covered by the simulation. In contrast, in the simulations that started with the NMR structure (panels d−f in Figure 5), the plateaus in the plots exist for both rings A and B (although at different time scales). These, therefore, allow us to conclude that spatial modes of van der Waals ring−base interactions between the MAG molecule and the RNA aptamer are stable and persisted over the course of the entire dynamics starting from the X-ray-derived structure, whereas they are more mobile starting from the NMR structure.

Conclusion

Binding to an RNA aptamer affects the electronic structure and conformation of the malachite green molecule upon forming a complex by two dominant interactions: electrostatic; base-stacking. The effects of electrostatic interactions on the MAG electronic structure were reported in our previous work.[16] In the current study we have evaluated the effect of base-stacking forces on the MAG−RNA interaction. These results show that one consequence of the binding of the MAG molecule to the

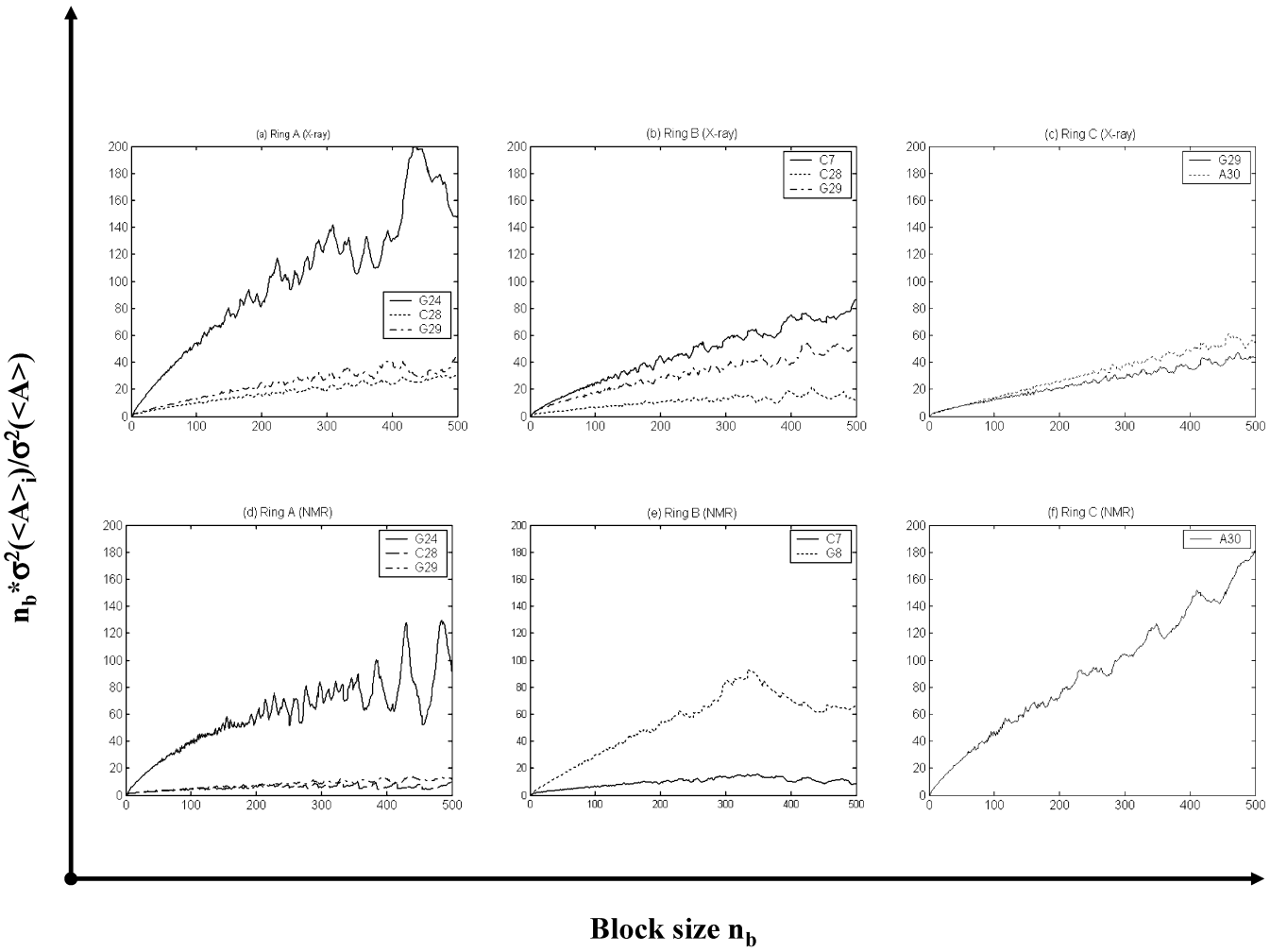

Figure 5. Plots of statistical inefficiency *s* versus block size in terms of number of snapshot saved periodically every 2.0 ps. Panels a−c represent the statistical inefficiency analyses of van der Waals energy of interactions between rings of MAG molecule with bases of the RNA aptamer, whose starting structure was determined by the X-ray technique for dominant peaks shown in Figure 4. Similarly, panels d−f represent the statistical inefficiency analyses of the MAG molecule with the RNA aptamer, whose structure was determined by NMR technique for dominant peaks shown in this figure.

RNA aptamer is that the rings of the MAG molecule adopt a more coplanar structure. This conformation leads to a more extended π-system in the MAG that we propose is the origin of the observed red-shift in its maximum absorption frequency upon binding to RNA. At the same time, the strength of binding of the dye to the RNA aptamer is correlated with its ability to form the coplanar conformation, as shown by a comparison of the binding energies of the MAG and TMR molecules to the RNA. Together with our previous work, we conclude that charges of the RNA backbone and surrounding counterions play an influential role in redistributing the electronic structure of the MAG molecule (causing an asymmetrical NMR chemical shift), while dispersive interactions with the RNA bases determine the binding strength, which correlates with the ligand structural flatness, causing the observed red-shift in the MAG's visible spectrum. These findings are important for understanding small molecule RNA interactions at the molecular level and as a basis for the rational design of molecules that interact specifically with RNA.

Acknowledgment. D.H.N. thanks Lawrence Livermore National Laboratory for the predoctoral fellowship (SEGRF) for partial support of this work and support from Professor Church at Harvard Medical School, where D.H.N is currently an Alfred P. Sloan and U.S. Department of Energy Postdoctoral Fellow in Computational Molecular Biology. This research was partially supported by the Office of Science (BER), U.S. Department of Energy, Grant No. DE-FG02-02ER63461, and was in part carried out at Lawrence Livermore National Laboratory under Contract W-7405-ENG-48 from the U.S. Department of Energy. T.D. acknowledges support from NSF Grant MCB 0110689.

Supporting Information Available: Appendix A, describing the MM-PBSA method and containing Tables A1 and A2 (binding energies and energy contributions), and Appendix B, describing statistical inefficiency and containing Figure B1 (plots of statistical inefficiency *s* versus block size). This material is available free of charge via the Internet at http://pubs.acs.org.

References and Notes

(1) Nahvi, A.; Sudarsan, N.; Ebert, M. S.; Zou, X.; Brown, K. L.; Breaker, R. R. *Chem. Biol.* **2002**, *9*, 1043−1049.

(2) Winkler, W.; Nahvi, A.; Breaker, R. R. *Nature* **2002**, *419*, 952−956.

(3) Winkler, W. C.; Cohen-Chalamish, S.; Breaker, R. R. *Proc. Natl. Acad. Sci. U.S.A.* **2002**, 99, 15908−15913.

(4) Hermann, T.; Westhof, E. *Curr. Opin. Biotechnol.* **1998**, *9*, 66−73.

(5) Hermann, T.; Westhof, E. *Comb. Chem. High Throughput Screening* **2000**, *3*, 219−234.

(6) Feigon, J.; Dieckmann, T.; Smith, F. W. *Chem. Biol.* **1996**, *3*, 611−617.
(7) Heus, H. A. *Nat. Struct. Biol.* **1997**, *4*, 597−600.
(8) Burgstaller, P.; Jenne, A.; Blind, M. *Curr. Opin. Drug Discovery Dev.* **2002**, *5*, 690−700.
(9) Sassanfar, M.; Szostak, J. W. *Nature* **1993**, *364*, 550−553.
(10) Dieckmann, T.; Suzuki, E.; Nakamura, G. K.; Feigon, J. *RNA* **1996**, *2*, 628−640.
(11) Patel, D. J.; Suri, A. K.; Jiang, F.; Jiang, L.; Fan, P.; Kumar, R. A.; Nonin, S. *J. Mol. Biol.* **1997**, *272*, 645−664.
(12) Dieckmann, T.; Butcher, S. E.; Sassanfar, M.; Szostak, J. W.; Feigon, J. *J. Mol. Biol.* **1997**, *273*, 467−478.
(13) Grate, D.; Wilson, C. *Proc. Natl. Acad. Sci. U.S.A.* **1999**, 96, 6131−6136.
(14) Baugh, C.; Grate, D.; Wilson, C. *J. Mol. Biol.* **2002**, *301*, 117−128.
(15) Flinders, J.; DeFina, S. C.; Baugh, C.; Wilson, C.; Dieckmann, T. *ChemBioChem* **2003**, in press.
(16) Nguyen, D. H.; DeFina, S. C.; Fink, W. H.; Dieckmann, T. *J. Am. Chem. Soc.* **2002**, *124*, 15081−15084.
(17) Kabsch, W. *Acta Crystallogr., Sect. A* **1976**, *32*, 922−923.
(18) Kabsch, W. *Acta Crystallogr., Sect. A* **1978**, *34*, 827−828.
(19) Jorgensen, W. L.; Chandrasekhar, J.; Madura, J. D.; Impey, R. W.; Klein, M. L. *J. Chem. Phys.* **1983**, *79*, 926−935.
(20) Case, D. A.; Pearlman, D. A.; Caldwell, J. W.; Cheatham, T. E., III; Ross, W. S.; Simmerling, C. L.; Darden, T. A.; Merz, K. M.; Stanton, R. V.; Cheng, A. L.; Vincent, J. J.; Crowley, M.; Tsui, V.; Radmer, R. J.; Duan, Y.; Pitera, J.; Massova, I.; Seibel, G. L.; Singh, U. C.; Weiner, P. K.; Kollman, P. A. *AMBER 6*; University of California: San Francisco, CA, 1999.
(21) Cornell, W. D.; Cieplak, P.; Bayly, C. I.; Gould, I. R.; Merz, K. M., Jr.; Ferguson, D. M.; Spellmeyer, D. C.; Fox, T.; Caldwell, J. W.; Kollman, P. A. *J. Am. Chem. Soc.* **1995**, *117*, 5179−5197.
(22) Essmann, U.; Perera, L.; Berkowitz, M. L.; Darden, T.; Hsing, L.; Pedersen, L. G. *J. Chem. Phys.* **1995**, *103*, 8577−8593
(23) Ryckaert, J. P.; Ciccotti, G.; Berendsen, H. J. C. *J. Comput. Phys.* **1977**, *23*, 327−341.
(24) Srinivasan, J.; Cheatham, T. E.; Cieplak, P.; Kollman, P. A.; Case, D. A. *J. Am. Chem. Soc.* **1998**, *120*, 9401−9409.
(25) Kollman, P. A.; Massova, I.; Reyes, C.; Kuhn, B.; Huo, S. H.; Chong, L.; Lee, M.; Lee, T.; Duan, Y.; Wang, W.; Donini, O.; Cieplak, P.; Srinivasan, J.; Case, D. A.; Cheatham, T. E. *Acc. Chem. Res.* **2000**, *33*, 889−897.
(26) Nguyen, D. H.; Colvin, M. E.; Yeh, Y.; Feeney, R. E.; Fink, W. H. *Biophys. J.* **2002**, *82*, 2892−2905.
(27) McCammon, J. A.; Harvey S. C. *Dynamics of proteins and nucleic acids*; Cambridge University Press: Cambridge, U.K., New York, 1987.
(28) Sinnokrot, M. O.; Valeev, E. F.; Sherrill, C. D. *J. Am. Chem. Soc.* **2002**, *124*, 10887−10893.
(29) Guckian, K. M.; Schweitzer, B. A.; Ren, R. X.-F.; Sheils, C. J.; Tahmassebi, D. C.; Kool, E. T. *J. Am. Chem. Soc.* **2002**, *122*, 2213−2222.
(30) Jacucci, G.; Rahman, A. *Nuovo Cimento Soc. Ital. Fis., D* **1984**, *D4*, 341−356.
(31) Berendsen, H. J. C.; Postma, J. P. M.; van Gunsteren, W. F.; DiNola, A.; Haak, J. R. *J. Chem. Phys.* **1984**, *81*, 3684−3690.
(32) Nguyen, D. H. Ph.D. Dissertation, University of California, Davis, CA, 2002.
(33) Gouda, H.; Kuntz, I. D.; Case, D. A.; Kollman, P. A. *Biopolymers* **2003**, *68*, 16−34.